# Removal of Cd(II) from aqueous solution by a hierarchical porous hydroxylapatite-carbon composite prepared with the biotemplate of stalk internodes of sugarcane tops

Huan Deng[a], Zongqiang Zhu[b,*], Yinian Zhu[c,*], Hui Ding[c], Yanhong Li[c], Ju Lin[c], Lihao Zhang[b]

[a]*College of Light Industry and Food Engineering, Guangxi University, Nanning 530004, China, Tel. +86 773 2536719; email: denghuan@glut.edu.cn*
[b]*Guangxi Key Laboratory of Environmental Pollution Control Theory and Technology, Guilin University of Technology, Guilin 541004, China, Tel./Fax: +86 773 3693255; emails: zhuzongqiang@glut.edu.cn (Z. Zhu), 08zhanglihao@163.com (L. Zhang)*
[c]*College of Environmental Science and Engineering, Guilin University of Technology, Guilin 541004, China, Tel. +86 773 5891059; Fax: +86 773 5895330; emails: zhuyinian@glut.edu.cn (Y. Zhu), 102015205@glut.edu.cn (H. Ding), lyh1685@163.com (Y. Li), linjucd@163.com (J. Lin)*

## ABSTRACT

The stalk internodes of sugarcane tops were used as the biotemplate to prepare a hydroxylapatite-carbon adsorbent with the hierarchical porous microstructure of sugarcane stalks (HAP/C-SS). The HAP/C-SS adsorbent retained the porous microstructure of sugarcane top stalks, which essentially consisted of micropores, mesopores and macropores originating from the cavities of vessels, parenchyma cells, sclerenchyma cells and pits. The specific surface area was estimated to be 8.52–28.44 m$^2$/g by the Brunauer–Emmett–Teller method and 5.63 m$^2$/g by the mercury porosimetry method. The HAP/C-SS showed an excellent removal performance for Cd(II) ions. The removal capacities were determined to be 10.89, 18.00 and 51.93 mg/g for the adsorption at the initial Cd(II) concentrations of 10, 20 and 50 mg/L, respectively, which were comparable with the adsorption capacities of the synthetic hydroxylapatite nanoparticles. The pseudo-second-order kinetic model and the Langmuir isotherm could very well fit the experimental data. The formation of the $(Cd_xCa_{1-x})_5(PO_4)_3(OH)$ solid solution through the coexisting ion exchange and dissolution–precipitation ($x = 0.03–0.17$) processes was the main mechanism for the Cd(II) adsorption onto the HAP/C-SS adsorbent.

*Keywords:* Sugarcane top; Stalk biotemplate; Hierarchical porous microstructure; Hydroxylapatite; Removal performance; Cadmium

## 1. Introduction

Cadmium is a non-essential and highly toxic element that has been recognized for its acute toxicity to aquatic, animal and human life even at very low concentrations. Harmful health effect due to cadmium is well documented and reported to cause diarrhoea, stomach problems, kidney damage, bone lesions, serious damage to respiratory systems and lung insufficiency, renal toxicity, cancer and hypertension [1–4]. Cadmium has been released to the environment through natural processes and anthropogenic activities in a variety of ways such as manufacturing and application of batteries, fossil fuel combustion, mining and smelting of nonferrous metals, metal electroplating and manufacturing of phosphate fertilizers [1–4]. The maximum Cd concentration in drinking water is recommended to be 0.003 mg/L after the WHO provisional guideline, and that was adopted by many countries [5].

* Corresponding authors.

Different methods have already been developed to eliminate Cd(II) from wastewater, including adsorption, reverse osmosis, ion exchange, chemical precipitation, nanofiltration, membrane separation, biological sequestration and microbial transformation [1–4]. However, the adsorption is one of the most efficient, promising and popular methods among all the available techniques due to its easy operation and high efficiency [3,4].

Many materials have been used as adsorbents for the Cd(II) fixation, for example, activated carbon [6–8], dried plant parts and agricultural waste biomass [1–4, 9–14], fly ash and charred biomaterials [10,15,16], modified biomaterials [3,14,17], natural and synthetic hydroxylapatite (HAP) nanoparticles [18–20]. Previous investigations indicate that HAPs can be used to effectively remove various metallic ions from liquid wastes and contaminated waters either by adsorption or coprecipitation, owing to the low cost and tremendous adsorption affinity and the low leaching of adsorbed cadmium from exhausted adsorbent [18–20]. Recently, nanomaterials have attracted a significant environmental attention because of the large specific surface area, enormous number of active sites and high reactivity [21]. Synthesis of the nano-HAP particles with high surface area can increase the loading capacity for practical application [21]. However, the separation of HAP nanoparticles from the treated effluent is difficult to perform, time-consuming and cost-prohibitive, which might result in some toxicological problems in the effluent. Moreover, the HAP particles with grain sizes <1 μm are not suitable for column application because of the significant hydraulic obstruction and possible clogging [21]. Especially, the presence of Cd(II) could result in a remarkable aggregation of HAP nanoparticles [22]. These difficulties can be solved by converting the hierarchical porous microstructures of bioorganic plants into adsorbent materials, which is an alternative adsorbent-producing process in comparison with the conventional powder manufacturing techniques [23,24]. Significant efforts have been taken to use pre-treated plant materials in preparing microcellular-designed ceramics, which showed the hierarchical porous microstructures like the negative duplication of the wood biotemplate [24]. The hierarchical porous adsorbents are advantageous in the case requiring interconnected porosity, for example, filters [25].

Sugarcane (*Saccharum officinarum* L.) is the world's most productive crop for sugar and ethanol production and is growing in the warm temperate to tropical areas of the world, such as Brazil, India, China, Thailand, Pakistan, Mexico, etc [26]. After harvesting, the sugarcane tops that contain less sucrose were usually wasted in the field [27]. Approximately 10,000 kg/ha of crop residue in the form of tops are produced during harvesting, which accounts for round 15% dry matter of the total plant [26,28,29]. The sugarcane's fibrous vascular system of an open network can remove water contaminants due to the low cost, non-toxicity and stable physical properties, high degree of porosity and large specific surface area [30].

The aim of this work was to use the discarded tops of harvested sugarcane as a potential raw material for the removal of Cd(II) ions from aqueous solution, which has never been tried before. In this work, the stalk internodes of sugarcane tops, a crop residual, were collected and used as microstructural biotemplates for preparing the hierarchical porous adsorbent of HAP-C (HAP/C-SS). The Cd(II) adsorption experiment was then made using the prepared adsorbent, which was concerned with the study of the influences of adsorption conditions, the adsorption isotherms and kinetics and the adsorption mechanism.

## 2. Materials and methods

### 2.1. Adsorbent preparation and characterization

#### 2.1.1. Preparation

The stalk internodes of sugarcane tops were collected, peeled and cut into cubes of about $1 \times 1 \times 1 \ cm^3$ size, which were then boiled in 5% $NH_3$ solution for 6 h to eliminate the extractable components of sugarcane stalk internodes including sugar, fats, fatty acid, tropolones, gums, etc. Simultaneously, lignocellulosic cell walls could be disrupted in diluted alkali solution by the hydrolyzing of uronic and acetic acid esters, by the dissolving of lignin, hemicellulose and silica, or by the swelling of cellulose [31]. The pre-treated sugarcane biotemplates of stalk internodes were then cleaned with pure water, dried at 80°C for 24 h, carbonized in a muffle furnace at 350°C for 3 h, and cooled to room temperature. After that, the pre-treated sugarcane biotemplates were dipped in the saturated limewater solution for 2 h, and then taken out and dipped in 0.02 mol/L $(NH_4)_2HPO_4$ solution for 2 h. This soaking–soaking procedure was repeated five times. Finally, the soaked sugarcane biotemplates were putted in a stainless steel retort and dried in a furnace at 50°C for 1 d. The biotemplates were then cooled to room temperature to obtain the hierarchical porous adsorbent with the sugarcane stalk internodes microstructure (HAP/C-SS).

#### 2.1.2. Characterization

The specific surface areas were measured by both the mercury porosimetry method (PoreMaster 60GT, Quantachrome, Boynton Beach, FL, USA) and the Brunauer -Emmett -Teller (BET) method (NOVAe1000, Quantachrome, Boynton Beach, FL, USA). A zeta potential analyzer (Zetasizer Nano ZS90, Malvern, UK) was used to determine the zeta potential. A diffractometer (X'Pert PRO, PANalytical B.V., Almelo, The Netherlands) was applied to record the powder X-ray diffraction (XRD) patterns of the HAP/C-SS materials before and after Cd(II) adsorption. The morphology and the surface chemical composition were analyzed by a scanning electron microscopy (SEM, Jeol JSM-6380LV, Japan Electron Optics Ltd., Tokyo, Japan) with an energy dispersive spectroscopy (EDS, IE350, Oxford Instruments, Oxford, UK). The X-ray photoelectron spectra (XPS) of the HAP/C-SS materials before and after Cd(II) adsorption were collected using a Thermo Scientific ESCALAB 250Xi (Waltham, MA, USA).

### 2.2. Adsorption experiments

Analytically pure cadmium nitrate $(Cd(NO_3)_2 \cdot 4H_2O)$, nitric acid $(HNO_3)$ and ultrapure water were used to prepare the aqueous Cd(II) solution. The batch adsorption experiments were made in 100 mL plastic centrifuge tubes by agitating a certain amount of HAP/C-SS in 50 mL Cd(II) solutions with an isothermal shaker at 25°C and 150 rpm for 24 h. All

solutions after adsorption were centrifuged at 4,000 rpm for 5 min and filtered through 0.22 μm micropore membranes, and then the residual aqueous elemental concentrations were analyzed by an inductively coupled plasma - optical emission spectrometer (Optima 7000DV, Perkin-Elmer Inc., Waltham, MA, USA) under the operating conditions after the instrument manual.

The influence of time and the adsorption kinetics were investigated by agitating 0.4 g HAP/C-SS in 50 mL of 10, 15, 20, 30, 50 and 75 mg/L Cd(II) solutions at 25°C and pH 5 in 100 mL centrifuge tubes at an agitation speed of 150 rpm. The aqueous sampling was carried out from different centrifuge tubes at the time intervals of 5, 10, 15, 20, 30, 45, 60, 120, 180, 240, 300, 360, 420, 480, 540, 720, 1,080 and 1,440 min. The influence of initial concentration and the adsorption isotherms were determined by agitating 0.4 g HAP/C-SS in 50 mL solutions of different Cd(II) concentrations (5, 10, 20, 30, 40, 50, 75, 100, 125, 150 and 200 mg/L) of the initial pH 5 at the constant temperatures of 25°C, 35°C and 45°C. Influence of pH was examined by agitating 0.4 g HAP/C-SS in 50 mL of 10, 20 and 50 mg/L Cd(II) solutions of various pHs (1, 2, 3, 4, 5, 6, 7 and 8) at 25°C. Influence of adsorbent dose was researched by agitating 0.05, 0.10, 0.15, 0.20, 0.25, 0.30, 0.35, 0.40, 0.45 and 0.50 g HAP/C-SS in 50 mL of 10, 20 and 50 mg/L Cd(II) solutions at pH 5 and 25°C. The HAP/C-SS materials with different particle sizes (un-pulverized chip [>3 mm], 0.841–0.4 mm [20–40 mesh], 0.4–0.25 mm [40–60 mesh], 0.25–0.177 mm [60–80 mesh], 0.177–0.149 mm [80–100 mesh], <0.149 mm [<100 mesh]) were applied to examine the influence of adsorbent grain size at 25°C and the initial Cd(II) concentration of 10, 20, 50 and 100 mg/L. As comparison, the carbonized sugarcane stalk (sugarcane stalk charcoal), pure HAP powder and commercial activated carbon were also tested in the experiment.

# 3. Results and discussion

## 3.1. Characterization of the adsorbent

### 3.1.1. X-ray diffraction

The recorded XRD pattern of the HAP/C-SS adsorbent before Cd(II) adsorption agreed well with the HAP in both diffraction peak position and intensity (Fig. 1). The recorded peaks at $2\theta = 25.88°, 28.68°, 32.04°, 39.62°, 46.64°, 49.52°$ and $53.19°$ corresponded to the (002), (210), (211), (130), (222), (213) and (004) reflection peaks of HAP (reference code 00-001-1008).

The diffraction peaks of cadmium HAP (reference code 00-014-0302) were recognized in the HAP/C-SS adsorbent after Cd(II) adsorption (Figs. 1 and 2). Due to the closeness of the Ca(II) (0.99 Å) and Cd(II) (0.95 Å) ionic radii, the formation of the isomorphic solid solution among calcium HAP and cadmium HAP is considered possible, that is, the isomorphic substitution of Cd(II) in HAP can lead to the formation of the $(Cd_xCa_{1-x})_5(PO_4)_3(OH)$ solid solution [32]. Furthermore, all the peaks were shifted to the higher diffraction angles which indicated that there had been a contraction in structure because of the exchange of larger Ca(II) ions with smaller Cd(II) ions in the HAP crystal [32].

Based on the comparison of the peak position and intensity, the XRD analysis of the HAP/C-SS adsorbent

after Cd(II) adsorption confirmed the formation of the $(Cd_xCa_{1-x})_5(PO_4)_3(OH)$ solid solution in which the Cd/(Cd+Ca) molar ratio was lower than 0.19 of $(Cd_{0.19}Ca_{0.81})_5(PO_4)_3(OH)$ [32]. The regular shift of the (211) and (002) peaks to the higher diffraction angles also showed that the Cd/(Cd+Ca) molar ratio ($x$) increased with the increasing of the initial cadmium concentrations up to 300 mg/L (Fig. 2).

### 3.1.2. SEM and EDS

Figs. 3(a) and (b) show the typical SEM images of the HAP/C-SS adsorbent in transverse and longitudinal directions, respectively. All these morphological characters were inherited from the bio-precursors of sugarcane stalks, which combined micropores, mesopores and macropores (Fig. 3). The hierarchical porous microstructure of HAP/C-SS is honeycomblike and very beneficial for water migration. No gaps were detected between carbonized sugarcane stalk fibre and HAP.

The path for water and solutes movement is fundamentally affected by the anatomy of sugarcane stalks [33,34]. Sugarcane stalks are composed of many vascular bundles and storage parenchyma. The storage parenchyma cells of sugarcane top stalks are thin-walled with the diameter of
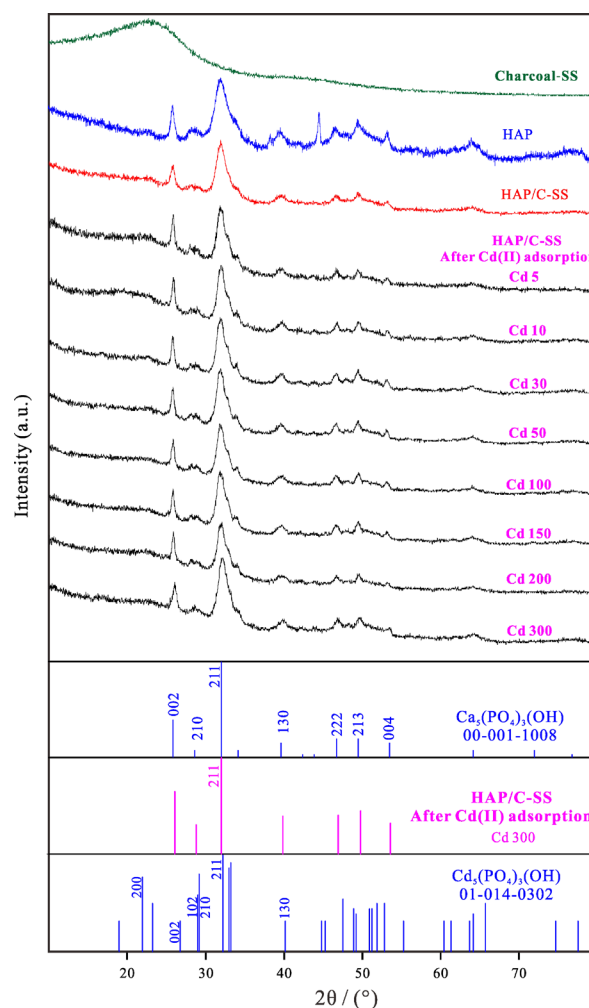


Fig. 1. XRD pattern of the HAP/C-SS adsorbent prepared with sugarcane stalk biotemplate before and after Cd(II) adsorption.
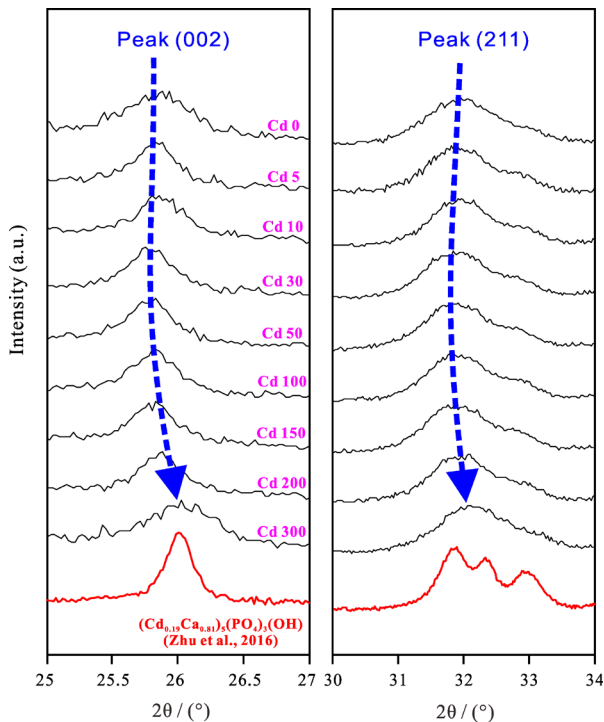
Fig. 2. Shift of the diffraction peaks (211) and (002) in the XRD pattern of HAP/C-SS after Cd(II) adsorption (initial concentration 300 mg/L; initial pH 5; adsorbent dose 0.4 g/50 mL; 25°C).

30–115 μm. The vascular bundles are collateral vessels with the diameter of 20–85 μm, which are enclosed in a sheath of lignified sclerenchyma thick-walled cells with the diameter of ~30 μm (Fig. 3).

Solution and solutes in the vascular bundles can move freely due to the symplasmical connection of all cell types. The flow capacity for water and solute movement among apoplastic compartments of sugarcane stalks can be reduced by the intensified lignification and suberization of the storage parenchyma cell walls in the later growing period [33,34]. Nevertheless, solution and solutes in the storage parenchyma cells can move freely within the apoplasts and symplasts through the nonlignified and nonsuberized cell walls, and through the plasmodesmata linking the abundant pits in the vessel and cell walls (Fig. 3). The stalk internodes of sugarcane tops are the growth apices and have the lowest degree of lignification and suberification, which is helpful for water and solute migration.

The EDS analysis showed that the HAP/C-SS adsorbent was composed of Ca, P, O and C, and the surface of the HAP/C-SS adsorbent after Cd(II) adsorption had a low Cd/(Cd+Ca) molar ratio of about 0.03–0.17 (Fig. 4).

### 3.1.3. X-ray photoelectron spectra

The XPS spectra result showed that the HAP/C-SS adsorbent contained Ca, P and O originating principally from the soaking limewater solution and $(NH_4)_2HPO_4$ solution, and carbon from the sugarcane stalk precursor (Fig. 5). After
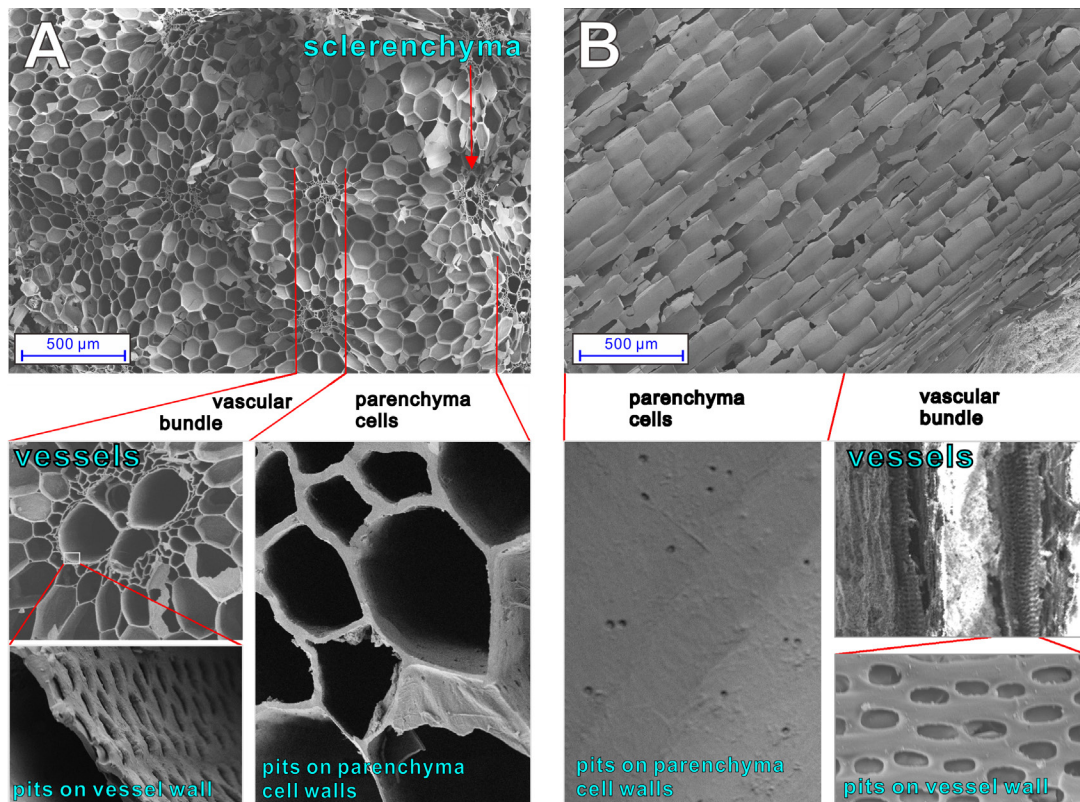


Fig. 3. SEM result of the HAP/C-SS adsorbent prepared with the stalk biotemplate of sugarcane top: (a) transverse direction and (b) longitudinal direction.

Cd(II) adsorption, the Cd3*d* peak in the spectrum was also detected. The shifts of the C, Ca, P and O peaks after Cd(II) adsorption were lesser than 0.05 eV, which indicated that the Cd(II) adsorption had no obvious influence on the state of calcium and phosphate on the adsorbent surface. Based on the peak areas of Ca2*p*, P2*p*, O1*s*, C1*s* and Cd3*d*, the component of the HAP/C-SS adsorbent after Cd(II) adsorption was calculated to be 2.51%, 3.27%, 16.14%, 77.60% and 0.48% for

Ca, P, O, C and Cd, respectively. The HAP/C-SS adsorbent had a Cd/(Cd+Ca) molar ratio of 0.16, which was within the EDS result of 0.03–0.17.

### 3.1.4. Surface area and pore size distribution

The hierarchical porous microstructure of the HAP/C-SS adsorbent combined the plentiful macropores, mesopores and micropores, which might result in well match between transport and ion adsorption [35,36].

The specific surface area of the HAP/C-SS adsorbent was measured to be 5.63 m²/g by the mercury porosimetry method. The porosity was determined to be 94.58% and the pore size changed from 0.0071 to 1,060 μm with the median pore diameter of 339.3 μm and the mean diameter of 15.73 μm (Fig. 6).

The nitrogen adsorption and desorption isotherms for the HAP/C-SS adsorbent belonged to the type-II curve with a type-H3 hysteresis loop after the empirical classification recommended by the International Union of Pure and Applied Chemistry (Fig. 7), which indicates a strong adsorbate–adsorbent interaction on the macroporous adsorbent and the
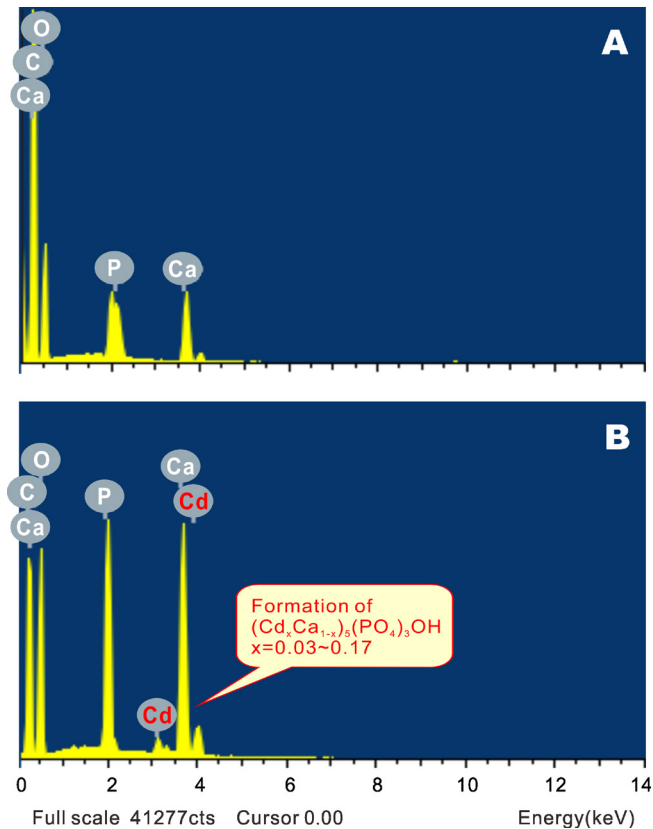


Fig. 4. EDS analysis result of the HAP/C-SS adsorbent prepared with the stalk biotemplate of sugarcane tops (a) before and (b) after Cd(II) adsorption.
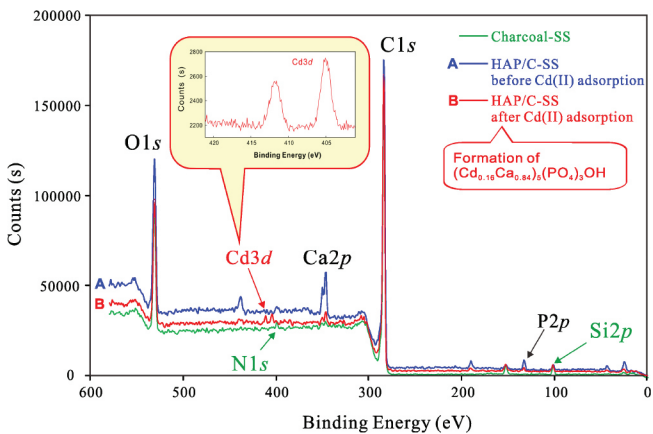


Fig. 5. XPS analysis result of the HAP/C-SS adsorbent prepared with the stalk biotemplate of sugarcane tops (a) before and (b) after Cd(II) adsorption.



| Mode Pore Diameter (μm) | 444.5 |
|---|---|
| Mean Pore Diameter (μm) | 15.73 |
| Median Pore Diameter (μm) | 339.3 |
| Specific Pore Volume (mL/g) | 22.15 |
| Specific Surface Area (m²/g) | 5.63 |
| Porosity (%) | 94.58 |
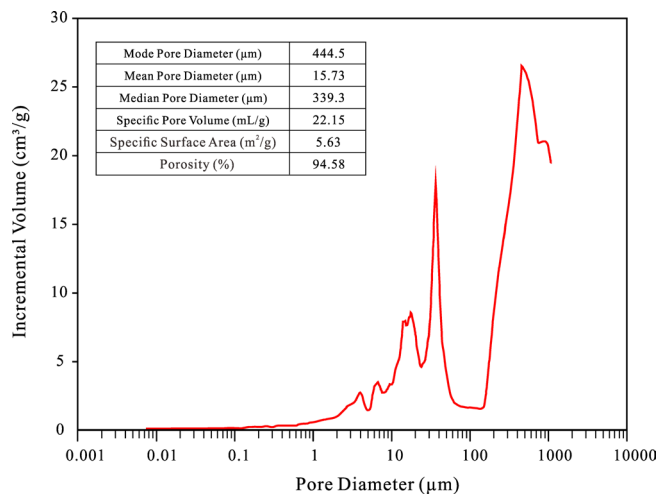
Fig. 6. Pore size distribution of the HAP/C-SS adsorbent from the Hg intrusion method.
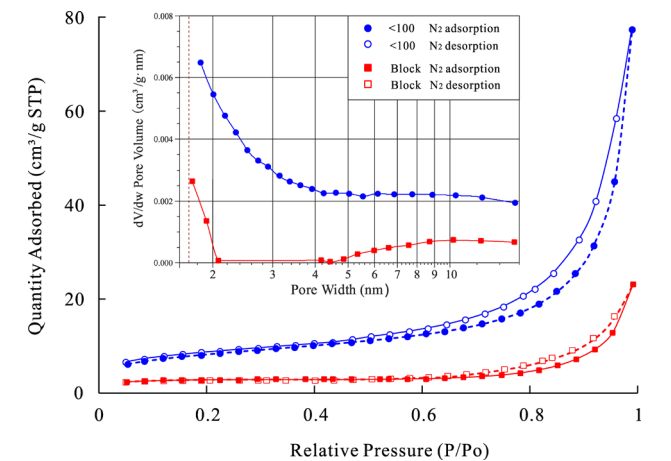


Fig. 7. Nitrogen adsorption isotherms of the HAP/C-SS adsorbent.

adsorbent with a type-H3 hysteresis possesses slit-shaped pores [36]. In addition, the volume change of the HAP/C-SS adsorbent might result in the low-pressure hysteresis (nitrogen in the relative pressure less than 0.4–0.45 at 77 K), for example, the swelling of non-rigid pores or the irreversible adsorption of the molecules in the pores of the same diameter as those of the adsorptive molecules [35]. The BET surface areas of the HAP/C-SS adsorbent with different grain sizes were calculated to be 8.52–28.44 $m^2$/g. The pore-size distribution showed the existence of the micro–meso–macroporous structure with a mean pore diameter of 5.39–7.43 nm (Fig. 7).

### 3.2. Influences of adsorption conditions

#### 3.2.1. Influence of contact time

The Cd(II) adsorption onto the HAP/C-SS adsorbent as a function of time is plotted in Fig. 8. Two different removal steps could be observed. The first step exhibited a fast Cd(II) removal, the second step was slow and quantitatively insignificant. The amount of Cd(II) adsorbed on the HAP/C-SS adsorbent increased and the residual aqueous Cd(II) concentrations decreased quickly with the contact time at the initial stage of adsorption, which showed a strong interaction between the adsorbent and Cd(II) ions (Fig. 8). The amount of Cd(II) adsorbed and the residual Cd(II) concentrations were

nearly steady after adsorption for 5 min at the initial pH of 5 and 25°C. For the initial Cd(II) concentrations of 10, 15, 20, 30, 50 and 75 mg/L, >90% of Cd(II) were adsorbed in 5 min at the mean adsorption rates of 0.1899, 0.4173, 0.4838, 0.8176, 1.1524 and 1.6989 mg/(g·min), respectively. The equilibrium time increased with the increase of the initial Cd(II) concentrations.

#### 3.2.2. Influence of initial concentration and temperature

The amount of Cd(II) adsorbed ($q_e$) and the removal rate vs. the initial Cd(II) concentrations are illustrated in Fig. 9. The general trends for the adsorption at different temperatures were alike. As the initial Cd(II) concentrations increased from 5 to 200 mg/L, the amount of Cd(II) adsorbed increased from 0.62 to 15.89 mg/g at 25°C, from 0.62 to 16.34 mg/g at 35°C, and from 0.62 to 23.62 mg/g at 45°C. Correspondingly, the adsorption removal rates decreased constantly from 98.53% to 61.53% at 25°C, from 98.45% to 63.34% at 35°C, and from 98.37% to 91.55% at 45°C. The Cd(II) removal efficiencies decreased as the initial Cd(II) concentrations increased due to the deficiency of available active sites required for the high initial Cd(II) concentrations. Nevertheless, the adsorption capacities of the HAP/C-SS adsorbent increased as the initial Cd(II) concentrations increased owing to the increasing mass transfer driving force and the increasing Cd(II) transfer rate from solution to the HAP/C-SS surface. The amount
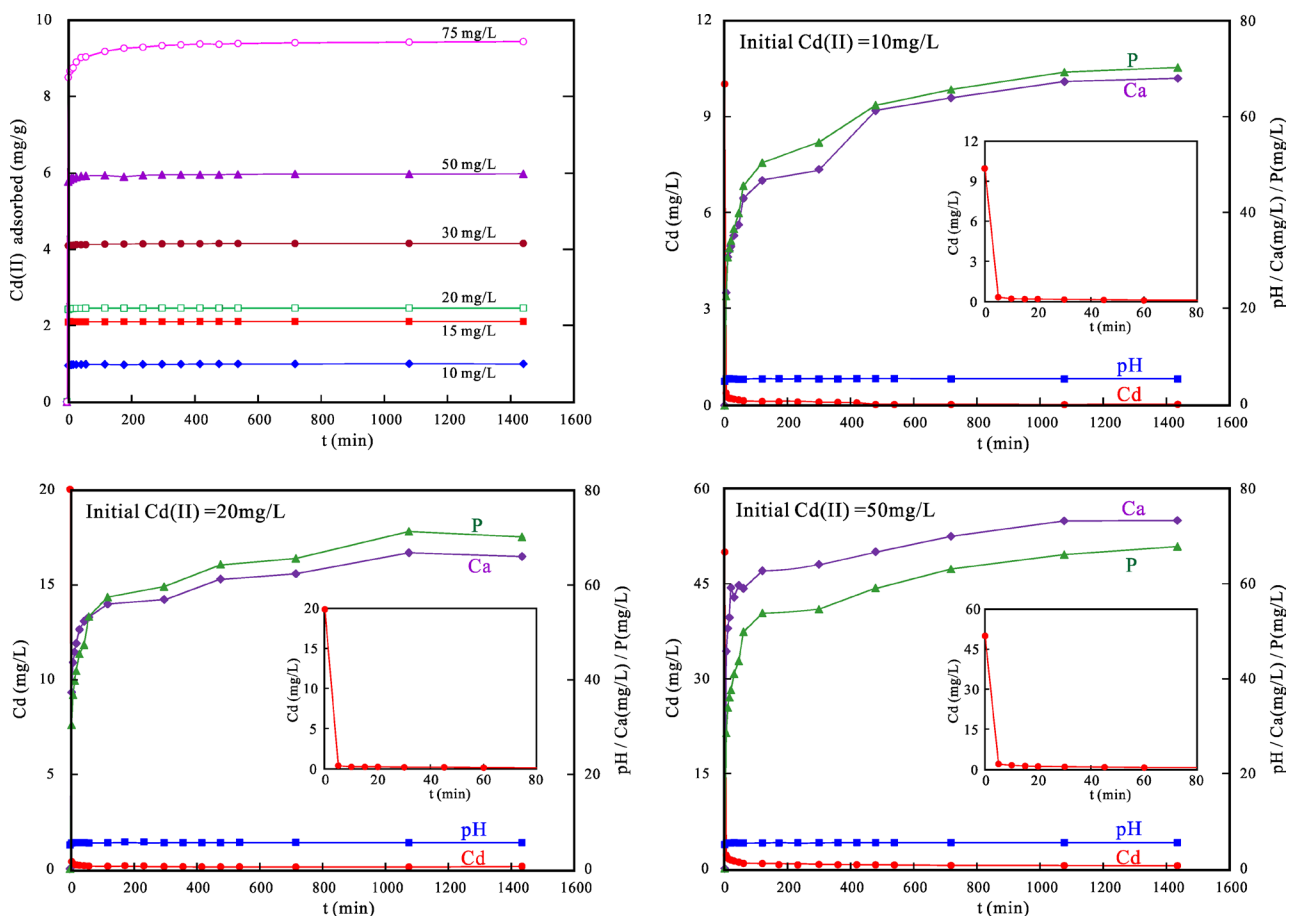


Fig. 8. Influence of contact time on Cd(II) adsorption onto the HAP/C-SS adsorbent (initial pH 5; adsorbent dose 0.4 g/50 mL; adsorbent grain size <100 mesh; 25°C).

of Cd(II) adsorbed ($q_e$) and the removal rate increased as the temperature increased, which suggested that the temperature could stimulate the Cd(II) adsorption and enable Cd(II) ions to diffuse rapidly through the HAP/C-SS adsorbent and the adsorption process was endothermic [22]. Because the influence of the adsorption temperature was negligible at the initial Cd(II) concentrations <50 mg/L (Fig. 9), 25°C was chosen in the following experiments.

### 3.2.3. Influence of initial solution pH

The solution pH is possibly the most important parameter governing the adsorption process [22]. Cd(II) ions could precipitate as hydroxides at pH > 9. Therefore, the influence of initial solution pH on the Cd(II) adsorption was studied over a pH range of 1–8. The amount of Cd(II) adsorbed onto the HAP/C-SS adsorbent ($q_e$) increased with the increase of the initial solution pHs up to 3–4 and approached a plateau at pHs > 3–4 indicating the existence of a second adsorption mechanism (Fig. 10). The adsorbent surface charge and the
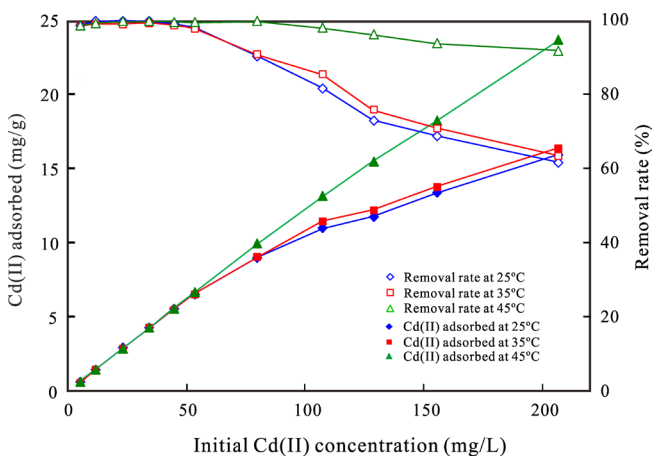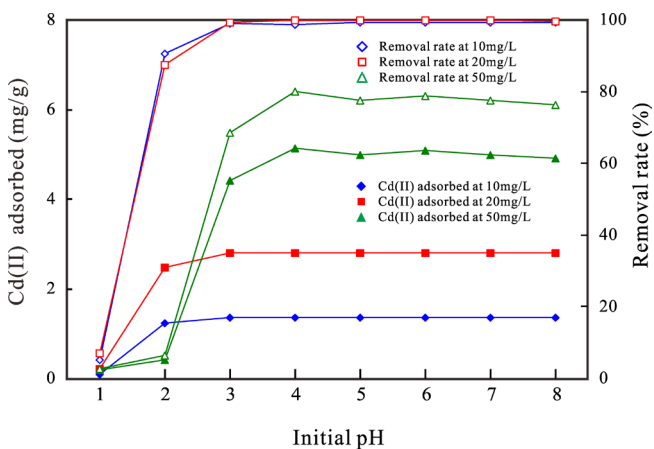
Cd(II) solution chemistry could be significantly influenced by the solution pH at the same time. The adsorption of the positively charged Cd(II) ions onto the HAP/C-SS surface was mainly affected by its surface charge that is dominated by the solution pH. High initial pH benefited the Cd(II) adsorption onto the HAP/C-SS adsorbent. For the initial Cd(II) concentration of 10–50 mg/L with pH > 3–4, most of the Cd(II) ions could be removed from the solution and the adsorption efficiency reached 76.21%–99.87%.

### 3.2.4. Influence of adsorbent dose

The adsorbent dosage controls the adsorption capacity for a given initial Cd(II) concentration. The total amount of Cd(II) adsorbed onto the HAP/C-SS adsorbent increased with the increasing adsorbent dose (Fig. 11), which was related to the availability of more binding sites owing to the increased adsorbent surface area [16]. With the increasing of the adsorbent dose from 0.05 to 0.5 g in 50 mL solution, the removal efficiencies for Cd(II) ions increased constantly from 94.30% to 99.43%, 78.51% to 99.12% and 97.21% to 98.99% for the initial Cd(II) concentrations of 10, 20 and 50 mg/L, respectively. The corresponding unit adsorption capacities for Cd(II) ions decreased from 10.89 to 1.16 mg/g, 18.00 to 2.29 mg/g and 51.93 to 5.29 mg/g with the increasing adsorbent dosage, which maybe induced by the increasing number of vacant adsorption sites provided by the increased adsorbent dosage [4].

### 3.2.5. Influence of adsorbent grain size

The adsorption capacity and the removal rate were dependent on the particle size of the HAP/C-SS adsorbent and the initial Cd(II) concentrations. The amounts of Cd(II) adsorbed on the un-pulverized HAP/C-SS adsorbent (>3 mm) were 1.42, 2.75, 6.18 and 11.48 mg/g for the initial Cd(II) concentrations of 10, 20, 50 and 100 mg/L, respectively (Fig. 12). The corresponding removal rates were calculated to be 99.37%, 99.27%, 94.14% and 85.75%. The pulverized HAP/C-SS adsorbent of <0.149 mm (<100 mesh) and the un-pulverized HAP/C-SS adsorbent possessed a greater adsorption efficiency than the



Fig. 9. Influence of initial concentration and temperature on Cd(II) adsorption onto the HAP/C-SS adsorbent (initial pH 5; adsorbent dose 0.4 g/50 mL; adsorbent grain size <100 mesh).



Fig. 10. Influence of initial pH on Cd(II) adsorption onto the HAP/C-SS adsorbent (initial concentrations 10, 20 and 50 mg/L; adsorbent dose 0.4 g/50 mL; adsorbent grain size <100 mesh; 25°C).
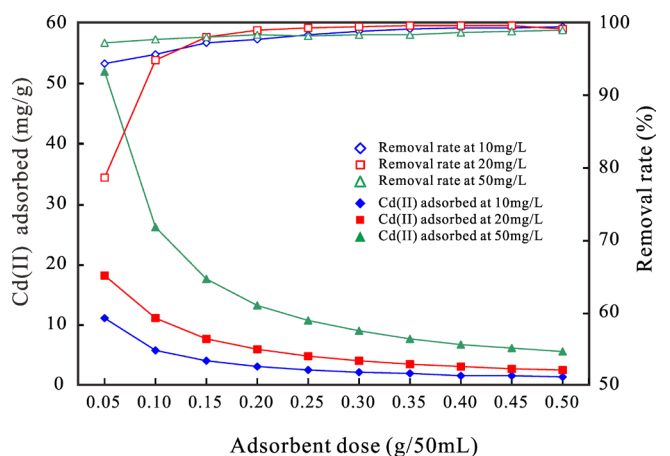


Fig. 11. Influence of adsorbent dose on Cd(II) adsorption onto the HAP/C-SS adsorbent (initial pH 5; initial concentrations 10, 20 and 50 mg/L; adsorbent grain size <100 mesh; 25°C).

sugarcane stalk charcoal and the mixture of the sugarcane stalk charcoal and HAP at different initial Cd(II) concentrations. For the adsorption at the initial Cd(II) concentrations of 10, 20, 50 and 100 mg/L, the pulverized HAP/C-SS adsorbent (<100 mesh) and the un-pulverized HAP/C-SS adsorbent showed a large adsorption capacity and a high removal rate that were comparable with the HAP powder.

For the initial Cd(II) concentration of 10–100 mg/L, the lowest adsorption capacity was determined to be 1.42–10.23 mg/g of the pulverized HAP/C-SS adsorbent (40–60 mesh or 0.4–0.25 mm) with the corresponding removal rate of 76.42%–99.60%. The highest adsorption capacity was found to be 1.42–12.91 mg/g of the pulverized HAP/C-SS adsorbent (<100 mesh or <0.149 mm) with the corresponding removal rate of 96.36%–99.85%. Comparatively, the un-pulverized HAP/C-SS adsorbent (chip, >3 mm) also had a high adsorption capacity (1.42–11.48 mg/g) and a large removal rate (85.75%–99.37%) owing to the hierarchical porous microstructure of the HAP/C-SS adsorbent prepared with sugarcane stalk biotemplate.

### 3.3. Adsorption kinetics and isotherm

#### 3.3.1. Adsorption kinetics

Among different kinetic equations, the experimental data could be best fitted to the pseudo-second-order kinetic equation that is described as following:

$$\frac{t}{q_t} = \frac{1}{k_2 q_e^2} + \frac{t}{q_e} \tag{1}$$

where $k_2$ is the pseudo-second-order constants (g/(mg·min)). The initial sorption rate ($h$) (mg/(g min)) can be computed with the following equation:

$$h = k_2 q_e^2 \tag{2}$$

The equilibrium adsorption capacity ($q_e$) and the pseudo-second-order constants ($k_2$) can be calculated from the slope and intercept of the straight line of plotting $t/q_t$ vs. $t$ (Fig. 13).

The correlation coefficients ($R^2 \approx 1.0000$) were closer to unity (Table 1), that is, the pseudo-second-order kinetic equation could be used to describe the Cd(II) adsorption onto the HAP/C-SS adsorbent perfectly, suggesting that the rate-limiting step is chemi-adsorption. The $k_2$ and $h$ values were 0.0430–2.3020 g/(mg·min) and 0.6816–13.8696 mg/(g·min), respectively (Table 1). The calculated adsorption capacities ($q_e$) (Table 1) were agreed very well with the actual values of 0.99, 2.10, 2.45, 4.15, 5.96 and 9.43 mg/g for the adsorption at the initial Cd(II) concentration of 10, 15, 20, 30, 50 and 75 mg/L, respectively.



Fig. 12. Adsorption of Cd(II) by the HAP/C-SS adsorbent (different grain sizes), the sugarcane stalk charcoal, pure HAP, commercial activated carbon and an 1:14 mixture of HAP and sugarcane stalk charcoal (initial pH 5; adsorbent dose 0.4 g/50 mL; 25°C).
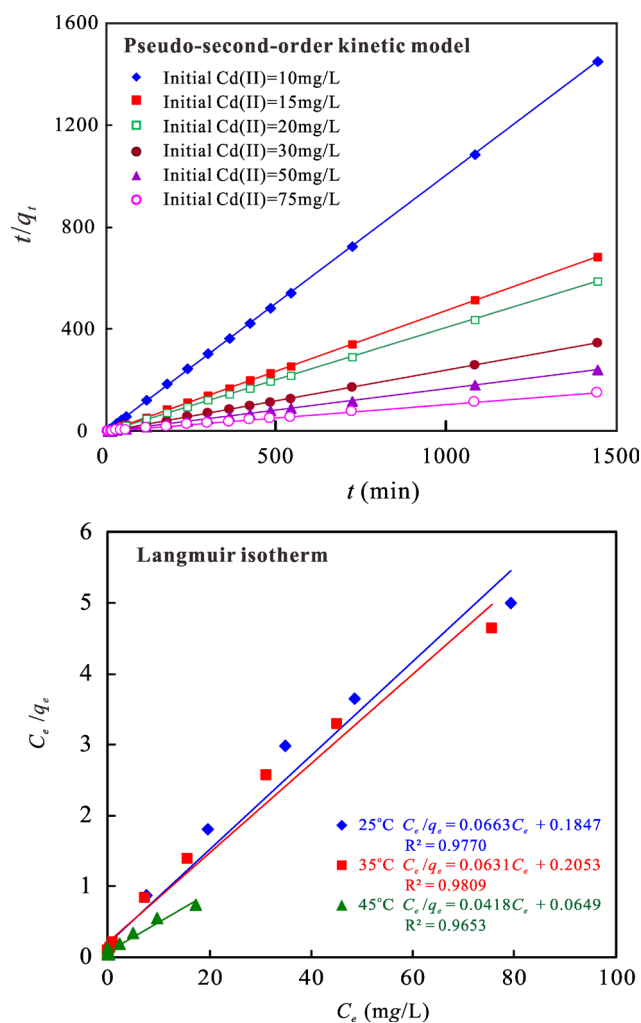


Fig. 13. Adsorption kinetics and isotherm for Cd(II) adsorption onto the HAP/C-SS adsorbent.

### 3.3.2. Adsorption isotherm

Langmuir adsorption isotherm is expressed as follows:

$$\frac{C_e}{q_e} = \frac{1}{(q_m \cdot K_L)} + \frac{C_e}{q_m} \tag{3}$$

where $C_e$ is the equilibrium Cd(II) concentration (mg/L), $q_m$ the adsorption capacity (mg/g) and $K_L$ the Langmuir constant (L/mg).

The linear plot of $C_e/q_e$ vs. $C_e$ indicated that the Cd(II) adsorption on the HAP/C-SS adsorbent followed the Langmuir isotherm (Fig. 13). The $q_m$ and $K_L$ constants were estimated from the regression line slopes and intercepts and are listed in Table 1.

The equilibrium constant or separation factor $(R_L)$ can be calculated to describe the nature of the Langmuir isotherm:

$$R_L = \frac{1}{(1 + K_L C_o)} \tag{4}$$

where $C_o$ is the initial Cd(II) concentration (mg/L).

The fitting result showed that the Langmuir isotherm yielded a good fit for the Cd(II) adsorption onto the HAP/C-SS adsorbent. The correlation coefficients $(R^2)$ were 0.9770, 0.9809 and 0.9653 for the adsorption at 25°C, 35°C and 45°C, respectively (Fig. 13 and Table 1). The high $R^2$ values indicated the homogeneous character of the adsorbent surface, where each adsorbate molecule is adsorbed onto the adsorbent surface with the same activation energy. The adsorption may be irreversible $(R_L < 0)$, linear $(R_L = 1)$, favourable $(0 < R_L < 1)$ or unfavourable $(R_L > 1)$. The $R_L$ values of 0.0075–0.3922 indicated a favourable adsorption for Cd(II) ions. The consistency obtained for the Langmuir isotherm is perhaps the initial indication of a possible ion-exchange on the HAP surface [22]. The Langmuir isotherm model fitted well the Cd(II) adsorption data, indicating a monolayer adsorption [37].

### 3.4. Comparison of the adsorption capacity of HAP/C-SS with sugarcane bagasse and HAP for Cd(II) removal

Table 2 presents a comparison of the HAP/C-SS adsorbent with some sugarcane bagasse and HAP adsorbents for the cadmium adsorption removal from water in literatures.

The Cd(II) adsorption capacity of the HAP/C-SS adsorbent was higher than that of the adsorbents prepared from sugarcane bagasse. The Cd(II) adsorption onto natural sugarcane bagasse was examined comprehensively. The Cd(II) adsorption capacities were determined to be 0.19–16.41 mg/g for natural sugarcane bagasse [1–4, 9–14], 0.62–47.48 mg/g for bagasse biochar and fly ash nanoparticles [10,15,16], 24.70–44.96 mg/g for activated carbon of sugarcane bagasse [6–8] and 1.92–46.46 mg/g for modified sugarcane bagasse [3,14,17].

The synthetic HAP adsorbents showed similar adsorption capacities for Cd(II) under similar adsorption condition. The Cd(II) adsorption capacities for synthetic HAP were determined to be 28.58 [38], 38.07 [39], 16.75 [40], 70.93 [41] and 41.70 mg/g [42].

Additionally, the maximum Cd(II) adsorption capacities of three commercial HAP adsorbents were measured to be 20.23 mg/g for the synthetic HAP from Merck KGaA (Darmstadt, Germany) [37], 48.78 mg/g for the synthetic HAP from Merck KGaA (Darmstadt, Germany) [22], 49.46 mg/g for the synthetic HAP from Bio-Rad (Hercules, CA, USA) [37] and 6.52–188.96 mg/g for the synthetic HAP from Alfa Aesar GmbH (Karlsruhe, Germany) [43].

The Cd(II) adsorption capacities of the HAP/C-SS adsorbent were 10.89, 18.00 and 51.93 mg/g for the initial Cd(II) concentrations of 10, 20 and 50 mg/L, respectively, which were comparable with the Cd(II) adsorption capacities of the synthetic HAP nano-adsorbents, for example, 64.07 mg/g for the synthetic nano-HAP [20], 56.37 mg/g for the synthetic nano-HAP [19] and 28.10 mg/g for the natural nano-HAP [18].

### 3.5. Adsorption mechanisms

The Cd(II) adsorption mechanism is a complex process. More than one step might be included in the

Table 1
Kinetics and isotherm parameters for Cd(II) adsorption onto the HAP/C-SS adsorbent

| Pseudo-second-order constants | | | | |
|---|---|---|---|---|
| Initial Cd(II) concentration (mg/L) | $k_2$ (g/(mg·min)) | $h$ (g/(mg·min)) | $q_e$ (mg/g) | $R^2$ |
| 10 | 0.6913 | 0.6816 | 0.99 | 1.0000 |
| 15 | 2.0702 | 9.1408 | 2.10 | 1.0000 |
| 20 | 2.3020 | 13.8696 | 2.45 | 1.0000 |
| 30 | 0.5148 | 8.8496 | 4.15 | 1.0000 |
| 50 | 0.1995 | 7.0922 | 5.96 | 1.0000 |
| 75 | 0.0430 | 3.8241 | 9.43 | 1.0000 |
| Langmuir constants | | | | |
| Temperature (°C) | $q_m$ (mg/g) | $K_L$ (L/mg) | $R_L$ | $R^2$ |
| 25 | 15.08 | 0.3590 | 0.0133–0.3559 | 0.9770 |
| 35 | 15.85 | 0.3074 | 0.0155–0.3922 | 0.9809 |
| 45 | 23.92 | 0.6441 | 0.0075–0.2354 | 0.9653 |

Table 2
Comparison of adsorption capacity of the HAP/C-SS composite with some other adsorbents for Cd(II) removal

| Adsorbent | pH | Concentration (mg/L) | BET surface area (m²/g) | Grain size (mm) | $T$ (°C) | Capacity (mg/g) | Reference |
|---|---|---|---|---|---|---|---|
| HAP/C-SS | 5 | 10–100 | 8.52 | >3 | 25 | 1.42–11.48 | This study |
| HAP/C-SS | 5 | 10–50 | 28.44 | <0.149 | 25 | 10.89–51.93 | This study[a] |
| HAP/C-SS | 5 | 10–100 | 28.44 | <0.149 | 25 | 1.42–12.91 | This study[b] |
| Charcoal-SS | 5 | 10–100 | – | <0.149 | 25 | 1.32–1.85 | This study |
| Activated carbon | 5 | 10–100 | – | <0.149 | 25 | 1.29–3.79 | This study |
| HAP powder | 5 | 10–100 | – | <0.149 | 25 | 1.42–13.15 | This study |
| Bagasse | 5–7 | 1–100 | – | 0.85 | 30 | 6.79 | [9] |
| Bagasse | 6 | 10 | – | <0.15 | Room | 0.58 | [10] |
| Bagasse | 6 | 5–500 | – | 0.15 | Room | 0.24–6.75 | [11] |
| Bagasse | 7 | 15 | – | ≤0.063 | 27 ± 1 | 5.33 | [12] |
| Bagasse | – | 0–2,000 | – | – | 25 | 1.15 | [13] |
| Bagasse | 4–7 | 50 | – | 0.15–0.11 | Room | 12.59 | [14] |
| Bagasse | 7 | 29.67–149.4 | – | <0.25 | 25 | 3.53 | [1] |
| Bagasse | 7 | – | 7.14 | <0.14 | Room | 0.19 | [2] |
| Bagasse | – | 10–30 | – | 0.25 | Room | 1.45 | [3] |
| Bagasse | 5 | 56.21 | – | <0.1 | Room | 16.41 | [4] |
| Bagasse biochar | 6 | 10 | – | <0.08 | Room | 0.62 | [10] |
| Bagasse fly ash | 4 | 100–500 | 66.17 | 0.075–0.09 | 30 | 47.48 | [15] |
| Bagasse fly ash | 6 | 2–20 | 210.8 | <0.25 | 20 ± 2 | 5.69 | [16] |
| Activated carbon of bagasse | 4.5 | 1–1,000 | 960 | <0.044 | 25 | 38.03 | [6] |
| Activated carbon of bagasse | 6 | 50 | 500.5 | 0.063–0.177 | 30 | 24.70 | [7] |
| Activated carbon of bagasse | – | 11.24–1349 | – | – | – | 44.96 | [8] |
| Bagasse modified with urea | 6 | 0.1–110 | – | <0.25 | 25 | 12.38 | [17] |
| Bagasse modified with EDTAD | 4–7 | 50 | – | 0.15–0.11 | Room | 46.46 | [14] |
| Bagasse modified with NaOH | – | 10–30 | – | 0.25 | Room | 2.14 | [3] |
| Bagasse modified with $HNO_3$ | – | 10–30 | – | 0.25 | Room | 1.92 | [3] |
| Bagasse modified with $H_2SO_4$ | – | 10–30 | – | 0.25 | Room | 2.221 | [3] |
| Activated carbon (Merck) | 6 | 50 | 284 | – | 30 | 16.05 | [7] |
| Natural HAP | 5.2–6.1 | 1.12–112.41 | 1.5 | 0.01–0.1 | 22 ± 2 | 28.10 | [18] |
| Synthetic HAP (Merck) | 6–7 | 10 | 52 | <0.0025 | 24.4 | 48.78 | [22] |
| Synthetic HAP (Merck) | 5 | 1.12–112.41 | 66 | <0.025 | 25 | 20.23 | [37] |
| Synthetic HAP (Bio-Rad) | 5 | 1.12–112.41 | 77 | 0.025–0.25 | 25 | 49.46 | [37] |
| Synthetic HAP (Alfa Aesar) | 7.04 | 10–500 | 50 | 0.01 | 25 ± 2 | 6.52–188.96 | [43] |
| Synthetic HAP | 5–7 | 56.21 | 21 | <0.01 | 25 | 16.75 | [40] |
| Synthetic HAP | – | 20–498 | 74 | 0.09–0.125 | 25 | 70.93 | [41] |
| Synthetic HAP | – | 783.50 | 35.7 ± 0.5 | 0.0004–0.036 | 10 | 38.07 | [39] |
| Synthetic HAP | 5.0 ± 0.1 | 112.41 | 67 | – | 20 ± 1 | 41.70 | [42] |
| Synthetic HAP | 5–8 | 30 | 100 | 0.004 | Room | 28.58 | [38] |
| Synthetic HAP | 6.25 | 0–180 | 71.8 | 0.0973 | 25 ± 2 | 56.37 | [19] |
| Synthetic HAP | 5.5 | 224.82 | 130 | 0.02–0.2 | 25 ± 2 | 64.07 | [20] |

[a]Adsorbent dose = 0.05 g/50 mL.
[b]Adsorbent dose = 0.4 g/50 mL.

adsorption process at the same time [44,45]. The adsorption kinetic results of this work are in accordance with those of previous studies [41,43]. The overall removal of Cd(II) ions by the HAP/C-SS adsorbent was considered to be a two-step mechanism. The first step was a fast kinetics process and involved the fast surface complexation of Cd(II) ions on the HAP/C-SS particles. The second step was a slow kinetics process, in which the diffusion of Cd(II) ions into additional adsorption sites within the HAP/C-SS particles occurred through the ion substitution of Cd(II) for Ca(II), resulting in the formation of the Cd-containing HAP solid solution $[(Cd_xCa_{1-x})_5(PO_4)_3(OH)]$ [41,43] and the increase

of the aqueous Ca(II) concentration with time (Fig. 8). This ion-exchange mechanism can be expressed as follows:

$$Ca_5(PO_4)_3(OH) + 5xCd^{2+} = 5xCa^{2+}$$
$$+ (Cd_xCa_{1-x})_5(PO_4)_3(OH) \tag{5}$$
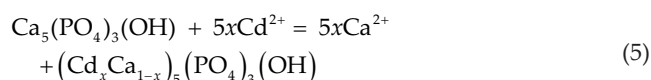
The surface complexation mechanism is supported by the XRD result as no secondary crystalline phase other than HAP was detected in the solid residues and the SEM observation that did not find any differences in the morphology of the solid residues in comparison to the original HAP/C-SS adsorbent, while the EDS and XPS analysis confirmed the existence of cadmium on the HAP/C-SS surface.

The adsorption equilibria are pH-dependent; therefore, the following protonation–deprotonation reactions must also be considered:

$$Ca_5(PO_4)_3(OH) = 5Ca^{2+} + 3PO_4^{3-} + OH^- \tag{6}$$

$$PO_4^{3-} + 3H^+ = HPO_4^{2-} + 2H^+ = H_2PO_4^- + H^+ = H_3PO_4^0 \tag{7}$$

$$Ca^{2+} + 2OH^- = Ca(OH)^+ + OH^- = Ca(OH)_2 \tag{8}$$
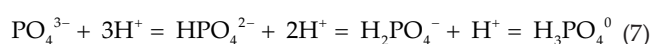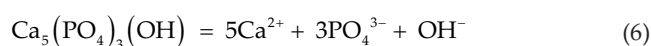
When the solution pH is greater than the $pH_{PZC}$ of the HAP/C-SS adsorbent (1.06), its surface charge is negative owing to the OH⁻ adsorption from solution, which will result in an increased electrostatic attraction force between the aqueous Cd(II) ions and the solid surface that contributes a more effective Cd(II) adsorption at higher pHs [40]. The percentage of different hydrolyzed Cd(II) species at a total Cd(II) concentration of 50 mg/L was computed using the following equilibrium constants by the PHREEQC program with the minteq.v4 database [46] and plotted as a function of pH in Fig. 14.

$$Cd^{2+} + H_2O = Cd(OH)^+ + H^+ \quad \log\_k = -10.097 \tag{9}$$

$$Cd^{2+} + 2H_2O = Cd(OH)_2^0 + 2H^+ \quad \log\_k = -20.294 \tag{10}$$

$$Cd^{2+} + 3H_2O = Cd(OH)_3^- + 3H^+ \quad \log\_k = -32.505 \tag{11}$$

$$Cd^{2+} + 4H_2O = Cd(OH)_4^{2-} + 4H^+ \quad \log\_k = -47.288 \tag{12}$$
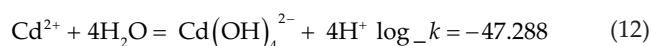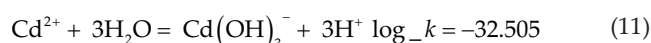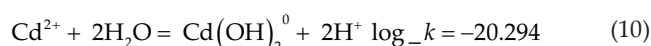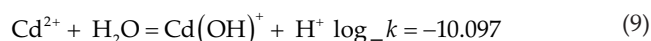
The removal capacity of the HAP/C-SS adsorbent increased with the increasing pH in acidic medium and remained constant in alkaline condition. This means that the positively charged $Cd^{2+}$ species were dominant at low pH and the adsorption on the HAP/C-SS adsorbent occurred at a faster rate. Nevertheless, there were some Cd(II) species with diverse charges like $Cd(OH)^+$, $Cd(OH)_2^0$, $Cd(OH)_3^-$ and $Cd(OH)_4^{2-}$ at high pH (Fig. 14).

As the dissolution of HAP, the $(Cd_xCa_{1-x})_5(PO_4)_3(OH)$ solid solution would precipitate according to the following reaction, which resulted in the formation of the $(Cd_xCa_{1-x})_5(PO_4)_3(OH)$ solid solution with relatively lower Cd/(Cd+Ca) molar ratio ($x < 0.19$).

$$5xCd^{2+} + (5-5x)Ca^{2+} + 3PO_4^{3-} + OH^-$$
$$= (Cd_xCa_{1-x})_5(PO_4)_3(OH) \tag{13}$$
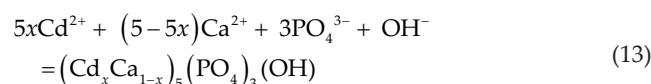
The solubility products ($K_{sp}$) were $10^{-64.62}$ for cadmium HAP ($Cd_5(PO_4)_3(OH)$) and $10^{-57.65}$ for calcium HAP ($Ca_5(PO_4)_3(OH)$). The solubility of the $(Cd_xCa_{1-x})_5(PO_4)_3(OH)$ solid solution decreased with increase of the Cd/(Cd+Ca) molar ratio ($x$) [32].

The saturation state can exert a significant effect on the nucleation and growth processes [47]. The saturation indexes (defined as the ratio of the ion activity product to the equilibrium solubility product) with respect to the $(Cd_xCa_{1-x})_5(PO_4)_3(OH)$ solid solution were calculated using the stability constants from Zhu et al. [32] to follow the dissolution–precipitation process (Fig. 15). The result indicated that the initial Cd(II) solution was firstly saturated with respect to the $(Cd_{0.19}Ca_{0.81})_5(PO_4)_3(OH)$ solid solution within 20 min, and then saturated with respect to the $(Cd_{0.09}Ca_{0.91})_5(PO_4)_3(OH)$ and $(Cd_{0.29}Ca_{0.71})_5(PO_4)_3(OH)$ solid solution after 120 min. After interaction for 480 min, the aqueous solution also had reached saturation with respect to pure calcium HAP ($Ca_5(PO_4)_3(OH)$). Finally, a solid phase
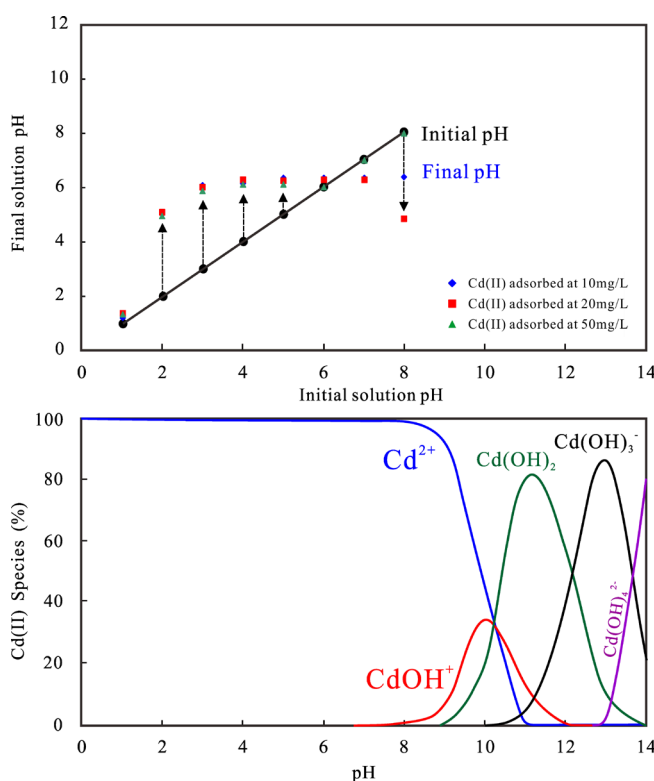


Fig. 14. Variation of the solution pH during Cd(II) adsorption onto the HAP/C-SS adsorbent.
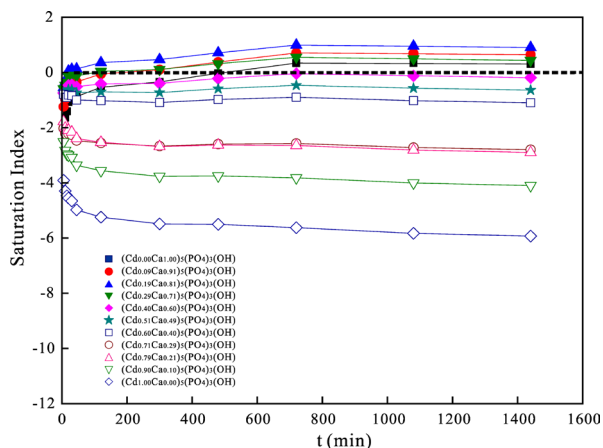
Fig. 15. Saturation index with respect to the $(Cd_xCa_{1-x})_5(PO_4)_3(OH)$ solid solution during Cd(II) adsorption onto the HAP/C-SS adsorbent (initial concentration 50 mg/L; initial pH 5; adsorbent dose 0.4 g/50 mL; 25°C).

with a component near $(Cd_{0.19}Ca_{0.81})_5(PO_4)_3(OH)$ would form due to the highest oversaturation of the aqueous solution with respect to $(Cd_{0.19}Ca_{0.81})_5(PO_4)_3(OH)$.

## 4. Conclusions

The prepared HAP/C-SS adsorbent inherited the hierarchical porous microstructure of sugarcane top stems and combined the abundant micropores, mesopores and macropores with a porosity of 94.58%, which originated from the cavities of vessels, parenchyma cells, sclerenchyma cells, pits, etc. Its specific surface area was estimated to be 5.63 m²/g through the mercury porosimetry method and 8.52–28.44 m²/g through the BET method.

The HAP/C-SS adsorbent showed an excellent removal performance for Cd(II) ions. The adsorption capacities were determined to be 10.89, 18.00 and 51.93 mg/g for the initial Cd(II) concentrations of 10, 20 and 50 mg/L, respectively, which were comparable with the adsorption capacity of the synthetic HAP nanoparticles. The experimental data could be very well fitted to the pseudo-second-order kinetic equation with the regression coefficients ($R^2$) near 1.0000. The adsorption followed Langmuir isotherm with the regression coefficients ($R^2$) >0.9653. The adsorption capacities ($q_e$) calculated from the models were also in consistent with the experimental data.

The Cd(II) adsorption onto the HAP/C-SS adsorbent was governed by two coexisting processes, that is, the ion exchange of Cd(II) for Ca(II) on the HAP/C-SS surface and the simultaneous formation of the $(Cd_xCa_{1-x})_5(PO_4)_3(OH)$ solid solution, and the partial dissolution of HAP and the following precipitation of the $(Cd_xCa_{1-x})_5(PO_4)_3(OH)$ solid solution with $x = 0.03–0.17$.

## Acknowledgments

## References

[1] X. Niu, L. Zheng, J. Zhou, Z. Dang, Z. Li, Synthesis of an adsorbent from sugarcane bagasse by graft copolymerization and its utilization to remove Cd(II) ions from aqueous solution, J. Taiwan Inst. Chem. Eng., 45 (2014) 2557–2564.

[2] M.S. Rosmi, S. Azhari, R. Ahmad, Adsorption of cadmium from aqueous solution by biomass: comparison of solid pineapple waste, sugarcane bagasse and activated carbon, Adv. Mater. Res., 832 (2014) 810–815.

[3] M. Mahmood-ul-Hassan, V. Suthar, E. Rafique, R. Ahmad, M. Yasin, Kinetics of cadmium, chromium, and lead sorption onto chemically modified sugarcane bagasse and wheat straw, Environ. Monit. Assess., 187 (2015) 1–11.

[4] J.X. Yu, L.Y. Wang, R.A. Chi, Y.F. Zhang, Z.G. Xu, J. Guo, Adsorption of Pb²⁺, Cd²⁺, Cu²⁺, and Zn²⁺ from aqueous solution by modified sugarcane bagasse, Res. Chem. Intermed., 41 (2015) 1525–1541.

[5] WHO (World Health Organization),Guidelines for drinking-water quality, 4th ed., 2017. Available at: http://apps.who.int/iris/bitstream/10665/254637/1/9789241549950-eng.pdf?ua=1.

[6] D. Mohan, K.P. Singh, Single- and multi-component adsorption of cadmium and zinc using activated carbon derived from bagasse – an agricultural waste, Water Res., 36 (2002) 2304–2318.

[7] K. Anoop Krishnan, T.S. Anirudhan, Removal of cadmium(II) from aqueous solutions by steam-activated sulphurised carbon prepared from sugar-cane bagasse pith: kinetics and equilibrium studies, Water SA, 29 (2003) 147–156.

[8] A. Coscione, B. Zini, Activated Carbon and Biochar from Agricultural By-products in the Adorption of Cd, Pb and Zn under Laboratory Conditions, Geophysical Research Abstracts 17, EGU General Assembly, Vienna, Austria, 2015.

[9] S.C. Ibrahim, M.A.K.M. Hanafiah, M.Z.A. Yahya, Removal of cadmium from aqueous solutions by adsorption onto sugarcane bagasse, Am. Eurasian J. Agric. Environ. Sci., 1 (2006) 179–184.

[10] M.E. Soltan, S.M. Sirry, E.M. Fawzy, Evaluation of the sorptive capacity of sugarcane bagasse and its coal for heavy metals in solution, J. Chin. Chem. Soc., 54 (2007) 1401–1412.

[11] U. Garg, M.P. Kaur, G.K. Jawa, D. Su, V.K. Garg, Removal of cadmium (II) from aqueous solutions by adsorption on agricultural waste biomass, J. Hazard. Mater., 154 (2008) 1149–1157.

[12] N.B. Isa, N.A.A. Wahab, M.R.H.M. Haris, Cd(II) removal from aqueous solution by unmodified sugarcane bagasse and coconut coir: adsorption equilibrium and kinetics, Int. Conf. Sci. Soc. Res., 4 (2010) 467–472.

[13] R.A. Sanchez, B.P. Espósito, Preparation of sugarcane bagasse modified with the thiophosphoryl function and its capacity for cadmium adsorption, Bioresources, 6 (2011) 2448–2459.

[14] Z. He, Y. Qi, J. Yu, R. Chi, Modified sugarcane bagasse for adsorption of Pb²⁺ and Cd²⁺, Environ. Sci. Technol., 35 (2012) 58–61 (in Chinese).

[15] B. Shah, C. Mistry, A. Shah, Seizure modeling of Pb(II) and Cd(II) from aqueous solution by chemically modified sugarcane bagasse fly ash: isotherms, kinetics, and column study, Environ. Sci. Pollut. Res., 20 (2013) 2193–2209.

[16] Z. Gholami, B. Ghorbani, A. Hooshmand, E. Moghbeli, Evaluation of modified bagasse fly ash nanoparticles on cadmium (II) removal from contaminated waters, Int. J. Agric. Innovations Res., 3 (2014) 379–384.

[17] B.L. Xiong, Y.L. Cui, J.Z. Zhang, M.X. Zhang, Investigation of the characteristics of adsorption of low-concentration Cd²⁺ and Cr³⁺ by modified sugarcane bagasse, J. Southwest Univ., 32 (2010) 118–123 (in Chinese).

[18] F. Fernane, M.O. Mecherri, P. Sharrock, M. Hdioui, H. Lounici, M. Fedoroff, Sorption of cadmium and copper ions on natural and synthetic hydroxylapatite particles, Mater. Charact., 59 (2008) 554–559.

[19] S.B. Chen, Y.B. Ma, L. Chen, K. Xian, Adsorption of aqueous $Cd^{2+}$, $Pb^{2+}$, $Cu^{2+}$ ions by nano-hydroxyapatite: single- and multi-metal competitive adsorption study, Geochem. J., 44 (2010) 233–239.

[20] Z. Zhang, M. Li, W. Chen, S. Zhu, N. Liu, L. Zhu, Immobilization of lead and cadmium from aqueous solution and contaminated sediment using nano-hydroxyapatite, Environ. Pollut., 158 (2010) 514–519.

[21] H. Guo, D. Stüben, Z. Berner, Removal of arsenic from aqueous solution by natural siderite and hematite, Appl. Geochem., 22 (2007) 1039–1051.

[22] S. Mandjiny, A.I. Zouboulis, K.A. Matis, Removal of cadmium from dilute solutions by hydroxyapatite, Sep. Sci. Technol., 30 (1995) 2963–2978.

[23] H. Sieber, Biomimetic synthesis of ceramics and ceramic composites, Mater. Sci. Eng., A, 412 (2005) 43–47.

[24] Z.Q. Zhu, Y.N. Zhu, H. Qin, Y.H. Li, Y.P. Liang, H. Deng, H.L. Liu, Preparation and properties of porous composite of hematite/magnetite/carbon with eucalyptus wood biotemplate, Mater. Manuf. Processes, 30 (2015) 285–291.

[25] M. Presas, J.Y. Pastor, J. Llorca, A.R. Arellano-López, J. Martínez-Fernández, R. Sepúlveda, Microstructure and fracture properties of biomorphic SiC, Int. J. Refract. Met. Hard Mater., 24 (2006) 49–54.

[26] J. Salinas-Chavira, L.J. Almaguer, C.E. Aguilera-Aceves, R.A. Zinn, M. Mellado, O. Ruiz-Barrera, Effect of substitution of sorghum stover with sugarcane top silage on ruminal dry matter degradability of diets and growth performance of feedlot hair lambs, Small Ruminant Res., 112 (2013) 73–77.

[27] G. Eggleston, M. Grisham, A. Antoine, Clarification properties of trash and stalk tissues from sugar cane, J. Agric. Food Chem., 58 (2010) 366–373.

[28] B.W. Mathews, C.J. Thurkins, Agronomic responses in the short-term to some management options for sugarcane top residue, J. Hawaiian Pac. Agric., 13 (2006) 23–34.

[29] S. Kumari, D. Das, Biologically pretreated sugarcane top as a potential raw material for the enhancement of gaseous energy recovery by two stage biohythane process, Bioresour. Technol., 218 (2016) 1090–1097.

[30] H. Nadaroglu, S. Cicek, A.A. Gungor, Removing Trypan blue dye using nano-Zn modified luffa sponge, Spectrochim. Acta, Part A, 172 (2017) 2–8.

[31] C.A. Rezende, M.A. de Lima, P. Mazier, E.R. de Azevedo, W. Garcia, I. Polikarpov, Chemical and morphological characterization of sugarcane bagasse submitted to a delignification process for enhanced enzymatic digestibility, Biotechnol. Biofuels, 4 (2011) 1–18.

[32] Y. Zhu, Z. Zhu, X. Zhao, Y. Liang, L. Dai, Y. Huang, Characterization, dissolution and solubility of cadmium–calcium hydroxyapatite solid solutions at 25°C, Chem. Geol., 423 (2016) 34–48.

[33] K.R. Jacobsen, D.G. Fisher, A. Maretzki, P.H. Moore, Developmental changes in the anatomy of the sugarcane stem in relation to phloem unloading and sucrose storage, Bot. Acta, 105 (1992) 70–80.

[34] C. Sant'Anna, L.T. Costa, Y. Abud, L. Biancatto, F.C. Miguens, W.D. Souza, Sugarcane cell wall structure and lignin distribution investigated by confocal and electron microscopy, Microsc. Res. Technol., 76 (2013) 829–834.

[35] S. Lowell, J.E. Shields, M.A. Thomas, M. Thommes, Characterization of Porous Solids and Powders: Surface Area, Pore Size and Density, Kluwer Academic Publisher, Boston, MA, USA, 2004.

[36] Z.A. Alothman, A review: Fundamental aspects of silicate mesoporous materials, Materials, 5 (2012) 2874–2902.

[37] F. Fernane, M.O. Mecherri, H. Lounici, M. Hadioui, Z. Harrache, Kinetic and sorption isotherms of cadmium, copper and nickel ions on two synthetic hydroxylapatites, J. Soc. Alg. Chim., 16 (2006) 127–138.

[38] R. Zhu, R. Yu, J. Yao, D. Mao, C. Xing, D. Wang, Removal of $Cd^{2+}$ from aqueous solutions by hydroxyapatite, Catal. Today, 139 (2008) 94–99.

[39] D. Marchat, D. Bernache-Assollant, E. Champion, Cadmium fixation by synthetic hydroxyapatite in aqueous solution – thermal behaviour, J. Hazard. Mater., 139 (2007) 453–460.

[40] I.D. Smičiklas, S.K. Milonjić, P. Pfendt, S. Raičević, The point of zero charge and sorption of cadmium (II) and strontium (II) ions on synthetic hydroxyapatite, Sep. Purif. Technol., 18 (2000) 185–194.

[41] N.C.C. da Rocha, R.C. de Campos, A.M. Rossi, E.L. Moreira, A. do F. Barbosa, G.T. Moure, Cadmium uptake by hydroxyapatite synthesized in different conditions and submitted to thermal treatment, Environ. Sci. Technol., 36 (2002) 1630–1635.

[42] I. Smičiklas, A. Onjia, S. Raicević, D. anaćković, M. Mitrić, Factors influencing the removal of divalent cations by hydroxyapatite, J. Hazard. Mater., 152 (2008) 876–884.

[43] A. Corami, S. Mignardi, V. Ferrini, Cadmium removal from single- and multi-metal (Cd+Pb+Zn+Cu) solutions by sorption on hydroxyapatite, J. Colloid Interface Sci., 317 (2008) 402–408.

[44] Y. Xu, F.W. Schwartz, S.J. Traina, Sorption of $Zn^{2+}$ and $Cd^{2+}$ on hydroxyapatite surfaces, Environ. Sci. Technol., 28 (1994) 1472–1480.

[45] I.D. Smičiklas, Cadmium immobilization by hydroxyapatite, Hem. Ind., 57 (2003) 101–106.

[46] D.L. Parkhurst, C.A.J. Appelo, Description of Input and Examples for PHREEQC Version 3 – A Computer Program for Speciation, Batch-Reaction, One-Dimensional Transport, and Inverse Geochemical Calculations, US Geological Survey Techniques and Methods, Book 6, Chapter A43, 2013, pp. 1–519.

[47] S.K. Lower, P.A. Maurice, S.J. Traina, E.H. Carlson, Aqueous Pb sorption by hydroxylapatite: applications of atomic force microscopy to dissolution, nucleation, and growth studies, Am. Mineral., 83 (1998) 147–158.

# Supplement A

The removal efficiency of cadmium ions in the presence of potentially interfering calcium and magnesium ions.
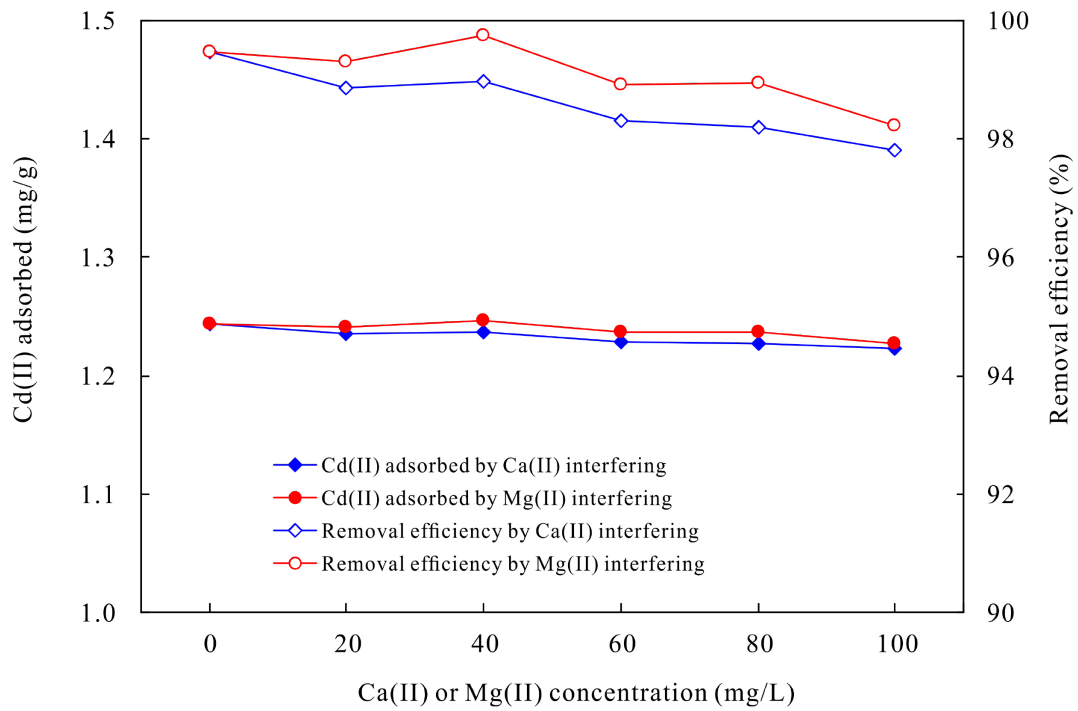


| Adsorption condition: |
|---|
| Ca(II) / Mg(II) concentration 0, 20, 40, 60, 80 and 100mg/L |
| Initial Cd(II) concentration 10mg/L |
| Initial Cd(II) solution pH 4 |
| Adsorbent grain size <100mesh |
| Adsorbent dose 0.4g/50mL |
| Temperature 25°C |
| Agitating 150rpm |
| Adsorption time 2h |

# Supplement B

The reusability of the HAP/C-SS adsorbent for removal of cadmium ions:
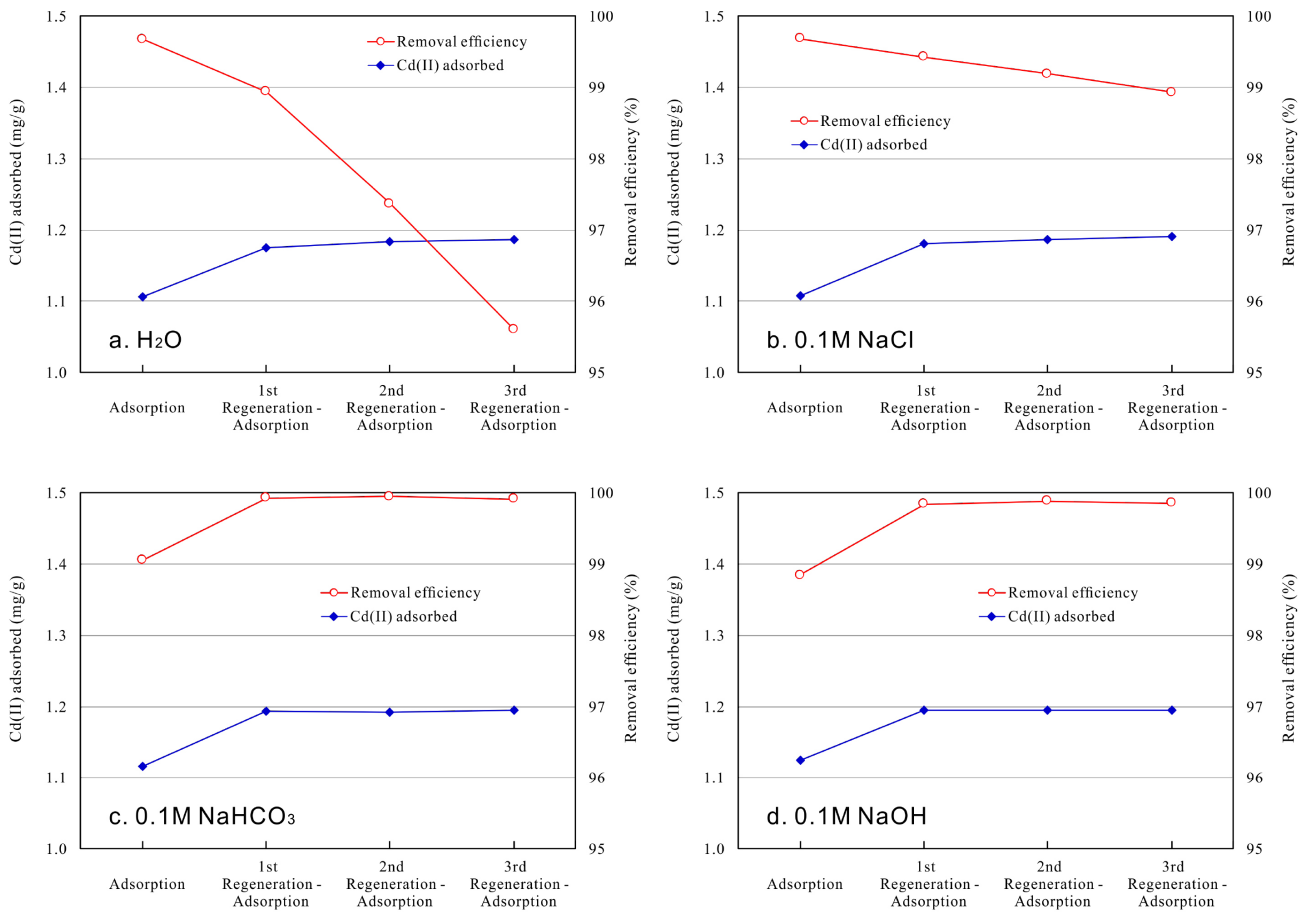


| Adsorption condition: | Regeneration condition: |
|---|---|
| Initial Cd(II) concentration 10mg/L | Regeneration solution $H_2O$ / 0.1M NaCl |
| Initial Cd(II) solution pH 4 | 0.1M $NaHCO_3$ / 0.1M NaOH |
| Adsorbent grain size <100mesh | Solution volume 50mL |
| Adsorbent dose 0.4g/50mL | Temperature 25°C |
| Temperature 25°C | Agitating 150rpm |
| Agitating 150rpm | Regeneration time 2h |
| Adsorption time 2h | |